Computationally motivated synthesis and enzyme kinetic evaluation of *N*-(β-D-glucopyranosyl)-1,2,4-triazolecarboxamides as glycogen phosphorylase inhibitors

Jaida Begum,[a] Gergely Varga,[b] Tibor Docsa,[c] Pál Gergely,[c] Joseph M. Hayes,*[a] László Juhász,*[b] László Somsák*[b]

[a]*Centre for Materials Science, Division of Chemistry, University of Central Lancashire, Preston PR1 2HE, United Kingdom*

[b]*Department of Organic Chemistry, University of Debrecen, POB 20, H-4010 Debrecen, Hungary*

[c]*Department of Medical Chemistry, Medical and Health Science Centre, University of Debrecen, Egyetem tér 1, H-4032 Debrecen, Hungary*

---

* Corresponding authors
tel: +3652512900 ext 22474 (LJ), 22348 (LS); fax: +3652512744; e-mail: juhasz.laszlo@science.unideb.hu, somsak.laszlo@science.unideb.hu
tel: +44172894334 (JMH), fax: +44172894981; email: jhayes@uclan.ac.uk

Abstract: Following our recent study of *N*-(β-D-glucopyranosyl)-oxadiazole-carboxamides (Polyák et al., Biorg. Med. Chem. 2013, 21, 5738) revealed as moderate inhibitors of glycogen phosphorylase (GP), *in silico* docking calculations using Glide have been performed on *N*-(β-D-glucopyranosyl)-1,2,4-triazolecarboxamides with different aryl substituents predicting more favorable binding at GP. The ligands were subsequently synthesized in moderate yields using *N*-(2,3,4,6-terta-O-acetyl-β-D-glucopyranosyl)-tetrazole-5-carboxamide as starting material. Kinetics experiments against rabbit muscle glycogen phosphorylase b (RMGPb) revealed the ligands to be low μM GP inhibitors; the phenyl analogue ($K_i = 1$ μM) is one of the most potent *N*-(β-D-glucopyranosyl)-heteroaryl-carboxamide-type inhibitors of the GP catalytic site discovered to date. Based on QM and QM/MM calculations, the potency of the ligands is predicted to arise from favorable intra- and intermolecular hydrogen bonds formed by the most stable solution phase tautomeric (**t2**) state of the 1,2,4-triazole in a conformationally dynamic system. ADMET property predictions revealed the compounds to have promising pharmacokinetic properties without any toxicity. This study highlights the benefits of a computationally lead approach to GP inhibitor design.

Keyword: 1,2,4-triazole, β-D-glucopyranosyl derivatives, glycogen phosphorylase, inhibitor, ADMET, docking, QM/MM

Introduction

Type 2 diabetes mellitus (T2DM) is characterized by hyperglycemia and peripheral insulin resistance, and represents more than 90% of all diabetic cases. The significant increase in the global incidence of diabetes is a major cause for concern, having doubled over the previous 3 decades to 347 million people in 2008.[1] Without adequate control of blood glucose levels, T2DM has several long term complications such as neuropathy and nephropathy, as well as an increased risk of blindness and cardiovascular disease.[2] Glycogen phosphorylase (GP; EC 2.4.1.1) is a validated target for T2DM having a direct influence on blood glucose levels through the glycogenolysis pathway.[3] It is an allosteric enzyme with a number of different binding sites,[4, 5] the catalytic, allosteric, new allosteric, inhibitor, glycogen storage, benzimiadazole[6] and the very recently identified quercetin binding site.[7] Significant efforts have been afforded to the design of GP inhibitors in recent years, with catalytic site inhibitors the most explored.[4, 8, 9] The physiological inhibitor of GP is α-D-glucose (K_i = 1.7 mM), but β-substitutions at the anomeric carbon of D-glucose have led to the most effective GP catalytic site inhibitors and have demonstrated blood sugar lowering effects *in vivo*.[10, 11]
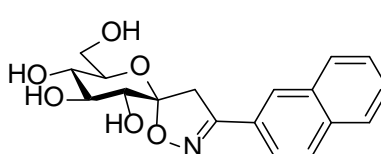

1a
K_i = 0˙16 μM

1b
K_i = 0˙35 μM

1c
K_i = 0˙41 μM
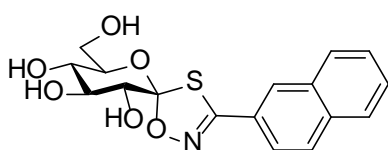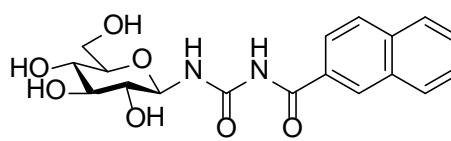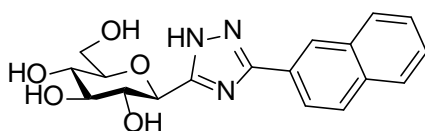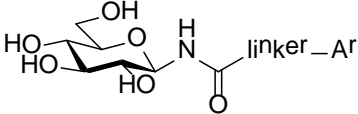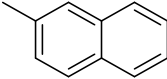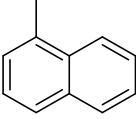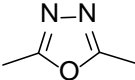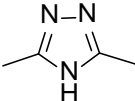
1d
K_i = 0˙63 μM

Figure 1. The four most potent glucose analogue inhibitors of GP discovered to date (**1a**,[12] **1b**,[5] **1c**[13, 14] and **1d**[15]) together with their K_i's for RMGPb inhibition. All ligands possess a 2-napthyl substituent exploiting favorable interactions in the GP catalytic site β–cavity.

An evaluation of the current status of β-D-glucopyranosyl analogues as GP inhibitors can be found in recent reviews.[4, 8] The four most potent discovered to date are shown in Figure 1, all of which possess a 2-napthyl moiety exploiting favorable interaction of aryl groups in the catalytic β-cavity, a pocket lined by both polar and non-polar groups. In general, the 2-napthyl moiety has proved the most effective in terms of potency, but our recent studies on *N*-(β-D-glucopyranosyl)-oxadiazole-carboxamides with linkers **2-4** (Table 1) have revealed that this is not always the case.[16] However, these ligands only demonstrated moderate potency at best, **2b** and **3c** the most potent with K_i's ~ 30 µM. The 1,2,4-triazole moiety in the form of 3-(β-D-glucopyranosyl)-5-substituted-1,2,4-triazoles has very recently revealed some of the most potent inhibitors of the GP catalytic si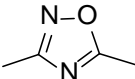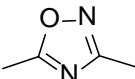te,[13, 14] with the 2-napthyl derivative (**1c** in Figure 1) the most potent. In the current work, we have investigated *N*-(β-D-glucopyranosyl)-3-substituted-1,2,4-triazole-5-carboxamides, replacing the oxadiazole moiety of linkers **2-4** with a 1,2,4-triazole (**5**, Table 1) in an attempt to improve ligand potency. Prior to undertaking synthesis, *in silico* calculations in the form of Glide docking, quantum mechanics (QM) and quantum mechanics/molecular mechanics (QM/MM) calculations were performed to probe the binding potential of these ligands at GP.

Table 1. Inhibition constants (K_i [μM], RMGPb) and Emodel docking scores from Glide (*in italics*) for *N*-(β-D-glucopyranosyl)-oxadiazole-carboxamides **2**-**4**, and *N*-(β-D-glucopyranosyl)-1,2,4-triazolecarboxamides **5**. The normalized values of Emodel are also shown in parentheses, as calculated using Eq. (1).

		Ar		
Linker	Scaffold	**a**	**b**	**C**
Oxadiazoles				
	2	545* *-92.31(-3.69)*	30 *-116.15(-4.01)*	172* *-112.17(-3.87)*
	3	136* *-100.68(-4.03)*	N.I.[a] *-115.78(-3.99)*	33 *-117.65(-4.06)*
	4	104 *-100.15(-4.01)*	N.I.[a] *-111.92(-3.86)*	145* *-113.96(-3.93)*
1,2,4-triazoles				
	5	1 *-102.34(-4.09)*	9.2 *-116.52(-4.02)*	- *-120.43(-4.15)*

[a] No inhibition. * Calculated from the IC_{50} values by the Cheng–Prusoff equation: $K_i = IC_{50}/(1 + [S]/Km)$.[17]
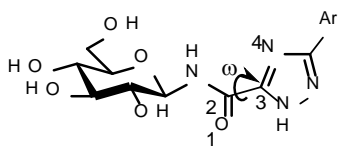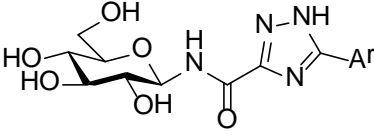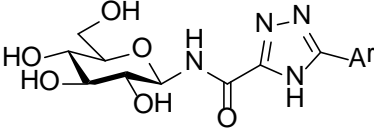
Results & Discussion

In Silico Binding Studies

All ligands in Table 1 were prepared for calculations using Maestro and the LigPrep 2.5 program[18] generating minimized favorable tautomeric and ionization states of all ligands at

pH = 7+/-2. All ligands were assigned as neutral, but three tautomeric forms (**t1**, **t2** and **t3**) of

the 1,2,4-triazole (linker **5**) were produced, with **t1** and **t2** the most probable based on LigPrep

with Epik (Table 2).[18] Monte Carlo conformational searches on models of ligands **5** and its

three tautomers **t1-t3** were performed followed by Jaguar 8.0 density functional theory (DFT)

with M06-2X[19] and the 6-31+G* basis set[20, 21](M06-2X/6-31+G*), and yielded the

conformations shown in Table 2. Higher level M06-2X/cc-pVTZ++[22] single point energy

(SPE) calculations in gas and solution phase at these geometries revealed that while **t1** is the

most favored in the gas phase by ~ 6 kcal/mol, **t2** is clearly preferred in solution (by ~ 9

kcal/mol). This is in contrast to the tautomeric probabilities from LigPrep/Epik, highlighting

the value of a QM approach to such analysis. Tautomer **t2** also allows for approximately two

equally stable conformations ($\omega = 0°$ or $180°$) in the free unbound solvated state, as defined by

the dihedral angle ω defined in Table 2. The molecular electrostatic potentials (MESPs) are

shown in Figure 2. For tautomer **t2,** the two different conformations have little effect on the

ESPs of the amide. However, the ESP in the space around a gas phase molecule is a key

factor in determining its ability to accept a proton; in this regard, for **t2** ($\omega = 180°$) the

maximum ESP of the triazole NH nitrogen (62.55 kcal/mol) and minimum ESP of the

connected N (-50.84 kcal/mol) is consistent with H^+ migration to form the most stable **t1**

tautomer in the gas phase (Table 2). The intra-molecular NH (amide) and triazole N (lone

pair) contacts for the tautomers can only loosely be classified as hydrogen bonds under the

current IUPAC guidelines[23] (donor angles are ~ 103-105°, hence less than the preferred >

110°), however, there is evidence of charge transfer in the case of **t1** and **t2** tautomers where

the magnitudes of the potential at the N are less ~ -15 kcal mol^{-1}. In any case, favourable

electrostatic stabilization occurs between these atoms and the contacts are present in all free

state conformations.   The conformational flexibility and MESP of **t2** compared to the other

tautomers become important factors when we consider the binding at GPb.

6

Table 2. Comparison of the relative energies (kcal/mol) of different tautomers and conformations of the 1,2,4-triazole (linker **5**) for models of the *N*-(β-D-glucopyranosyl)-1,2,4-triazolecarboxamides, as calculated using density functional theory. For simplicity and speed, in the calculations the β-D-glucopyranose was replaced by a methyl group and a phenyl used for the Ar group. Geometries used in calculations were from M06-2X/6-31+G* optimizations.[a]

Tautomer	Dihedral Angle ω (°)[b]	LigPrep Tautomer Probability	Gas Phase[c] M06-2X/ 6-31+G*	Gas Phase[c] M06-2X/ cc-pVTZ++	Solution Phase[c,d] M06-2X/ cc-pVTZ++
t1	180	0.487	0.0(0.0)[e]	0.0	8.6
t2	0 180	0.487	6.5(7.2)[e] 5.9(6.9)[e]	5.9 5.3	0.5 0.0
t3	0	0.027	5.9(6.4)[e]	5.5	9.0

[a] Tautomeric states were determined using LigPrep.[18] MacroModel 9.9[18] conformational searches were used to locate the above favorable conformations of the compounds, which were then used in the QM optimizations. The dihedral angle ω adopted by the atoms 1, 2, 3, 4 for rotation around the 2,3 bond is key to the conformational properties. [b] Values for the minima from the M06-2X/6-31+G* optimizations. [c] Single point energy calculations at the optimized M06-2X/6-31+G* geometries. [d] Continuum treatment of solvation which involved accurate numerical solution of the Poisson-Boltzmann (PBF) equation.[24, 25] [e] Relative Gibbs free energies given in parentheses.
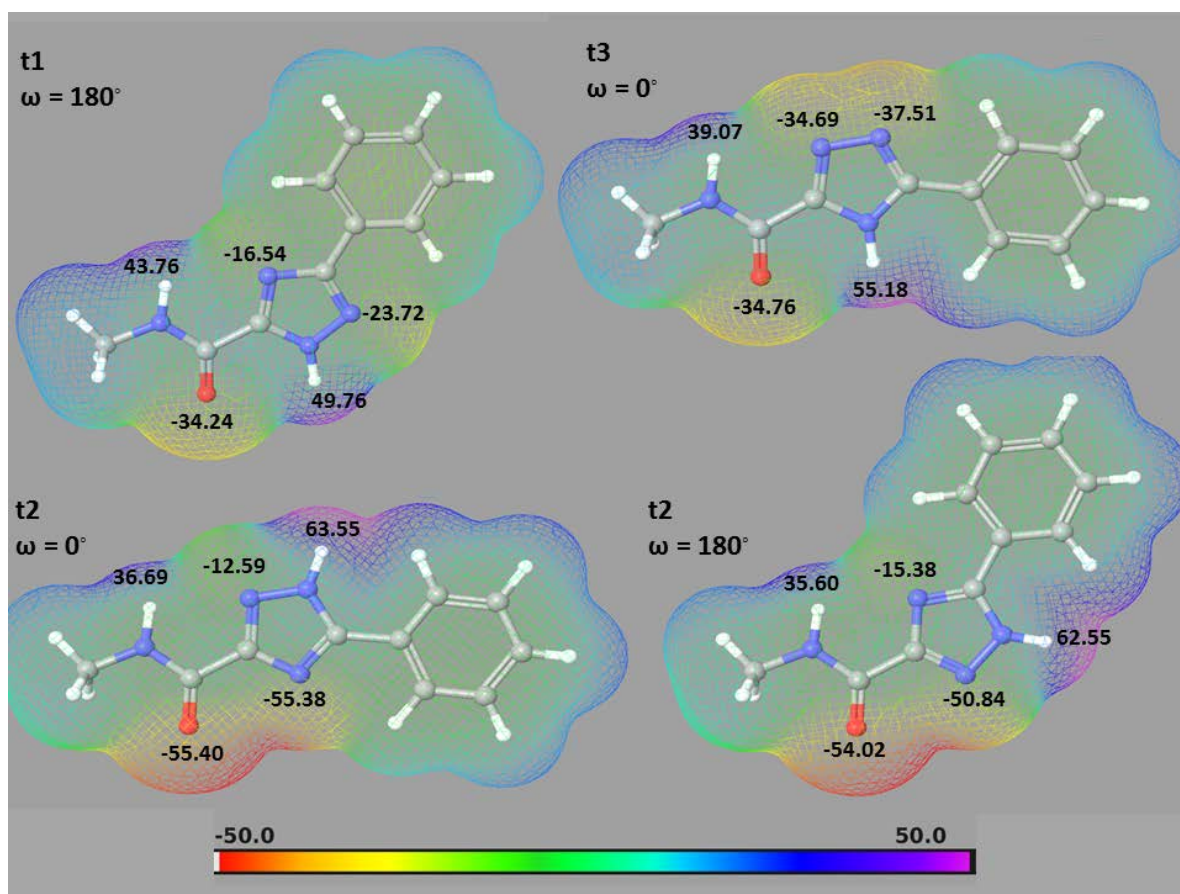
Figure 2. Molecular electrostatic potential (MESPs) can be used to provide insight into a number of hydrogen bonding phenomena. Shown are the results of MESP calculations (M06-2X/6-31+G*) on a model of the isolated **5a** ligand (Me groups instead of glucopyranose) in its different tautomeric forms and most stable conformations (Table 2). The electrostatic potentials are mapped onto the electron density surface for each molecule. Only the ESP range of -50–50 kcal mol^{-1} is used for a better visual demonstration of the tautomeric effects; actual minimum–maximum ESP values were -55.4 – 63.7 kcal mol^{-1} obtained for the **t2** tautomer. The minimum or maximum local electrostatic potential values (kcal/mol) for the relevant atoms are also shown.

Docking calculations were performed using Glide 5.8 in extra-precision (XP) mode,[18, 26] a docking algorithm which has proved effective in previous GPb catalytic site studies.[15, 27, 28] The predictive capability of Glide-XP in the current study was measured by the ability of the algorithm to reproduce the trends in the kinetics results for the *N*-(β-D-glucopyranosyl)-oxadiazole-carboxamides with linkers **2-4**. The results are shown in Table 1, with the most

consistent results obtained using the Emodel scoring function which combines GlideScore, the non-bonded interaction energy and the excess internal energy of the generated ligand conformation. Non-bonded interactions in a scoring function are typically calculated as a sum of pair-wise interactions. Hence, a larger compound often receives a more favorable score than a smaller compound. In order to overcome this bias, a number of different normalization and scaling approaches have been proposed.[29, 30] Given that the aforementioned trend appeared to occur for our training set ligands, we used the following equation to account for the different sizes of our aryl substituents (phenyl versus napthyl):

$$Emodel_{norm} = Emodel/number\ of\ heavy\ atoms \qquad\qquad Eq.(1)$$

On initial inspection of Table 1, the predictive capability of the docking does not appear obvious. For example, the score for **3b** is clearly over-estimated. However, a reasonable correlation $R^2 = 0.67$ between predicted ($Emodel_{norm}$) and experimental ($\ln K_i$) binding strengths was obtained. Further, the most favorable aryl group for each of the linkers **2-4** was correctly predicted: 2-napthalene (**2b**) in the case of **2**, 1-napthalene (**3c**) in the case of **3** (1-napthalene) and phenyl (**4a**) in the case of **4**. In terms of our key objective, to accurately predict the potential of linker **5**, we noted that the most favorable linker (from **2-4**) for each aryl group was also correctly identified: linker **2** in the case of 2-napthalene ($K_i = 30\ \mu$M), linker **3** for 1-napthalene ($K_i = 33\ \mu$M), and for phenyl the linkers **3** and **4** were predicted to have similar efficiency in line with kinetics (K_i's = 104-136 μM). *Encouraged by this, we then noted that for each of the phenyl, 1- and 2-naphthalence substituents, linker **5** was predicted to give rise to more potent ligands.*

Despite their obvious importance, tautomeric states are still often not accurately considered in computer-aided drug design efforts.[31] The most favorable tautomeric state for binding of ligands **5a-5c** based on Emodel docking scores was **t2** for both **5a** and **5c**, and **t1** for **5b** (Table 3). The potential of using the lowest QM/MM complex energy for protein-ligand

9

docking pose selection has recently been highlighted, where QM/MM energies were used to re-rank docking poses and compared with their native crystallographic binding modes.[32] Accordingly, to more accurately probe the binding of **5a-5c** and its different tautomers at GP, QM/MM optimizations with QSite 5.8 [18] were performed on the Glide docking poses (Table 3). M06-2X/6-31+G* was used for the QM region (the ligands), while the GPb protein was described using MM with the OPLS-AA(2005) forcefield,[33] with otherwise default options. Solution phase energies at the optimum geometries were then obtained, employing a self-consistent reaction field (SCRF) continuum treatment for water solvation effects and which involved accurate numerical solution of the Poisson-Boltzmann (PBF) equation (M06-2X/6-31+G* + PBF).[24, 25] The results of the QM/MM calculations (Table 3) revealed the most stable free state solution phase **t2** tautomer of **5a**-**5c** to also form the most favorable complexes with GPb, in both gas and solution phases. From the MESPs (Figure 2) also, the **t2** maximum and minimum atomic ESPs of the triazole NH nitrogen and amide CO oxygen (both conformations) are indicative of greater H-bond acceptor and donor capabilities,[34, 35] respectively, for binding at GPb compared to the other tautomers, although the value of ESP maxima on molecular surfaces for predicting hydrogen bond acidity has recently been questioned.[36]

Table 3. QM/MM gas and solution phase relative energies (kcal/mol) for the optimized Glide docking poses of ligands **5a**-**5c** considering the different tautomeric forms as described in the text. The corresponding Emodel docking scores are also shown.

Ligand	Tautomer[a]	Emodel (Emodel$_{norm}$)[b]	ω dihedral angle($°$)[c]	QM/MM relative energies	
				Gas Phase	Solution Phase
5a	**t1**	-99.8 (-3.99)	34.3	16.6	18.1
	t1	-93.9 (-3.76)	178.0	7.7	19.6
	t2	-102.3 (-4.09)	19.7	3.8	0.0
	t2	-97.1 (-3.88)	-176.7	0.0	10.7
	t3	-91.0 (-3.64)	3.5	14.5	13.3
5b	**t1**	-116.5 (-4.02)	33.3	14.5	15.8
	t2	-115.4 (-3.98)	-10.1	0.0	0.0
	t3	-115.9 (-4.00)	3.2	13.0	8.9
5c	**t1**	-114.3 (-3.94)	16.2	18.9	16.5
	t2	-120.4 (-4.15)	43.3	6.5	1.3
	t2	-114.6 (-3.95)	-10.7	0.0	0.0
	t3	-112.2 (-3.87)	-0.5	13.8	13.1
	t3	-110.5 (-3.81)	-154.9	11.8	6.4

[a] *c.f*. Table 2. [b] Normalized values as calculated using Eq. (1). [c] Numbering scheme for dihedral angle ω as shown in Table 2.

For the GPb-**5a** complex (Figure 3), as well as forming the standard hydrogen bonding interactions from the β-D-glucopyranosyl hydroxyl groups and a hydrogen bond from the carboxamide carbonyl O with the Leu136 backbone NH, through rotation around the dihedral angle ω the 1,2,4-triazole in its favored solution phase **t2** tautomeric form has the potential to hydrogen bond with the Asp339 carboxylate on one side of the β-cavity (water-bridged), and on the other side directly with the Asp283 backbone O (ω ~ 50°). If ω ~ 0° or ω ~ +/-180°, although the 1,2,4-triazole NH forms no direct hydrogen bonds with GPb, there are favorable intra-molecular interactions from the carboxamide NH with the lone pair of electrons on a triazole N atom for both conformations, as mentioned earlier for the free state ligand (Figure 2). The smaller Ar group (phenyl) of **5a** also permits a flipped 1,2,4-triazole conformation (ω = -176.7°) shown in Figure 4, where the triazole NH is a little longer than hydrogen bonding distance from the Glu88 sidechain carboxylate (distance ~ 3.3 Å). Hence, **5a** in its **t2** tautomeric state exhibits considerable conformational flexibility while bound at GPb (favorable in terms of entropy). The 1,2,4-triazole has either intra- and intermolecular hydrogen bonding potential in these different conformations; while CH-π interactions from the Asp283 CH to the ligand Ar (phenyl) group can further stabilize the GPb-**5a** complex (Figure 3). For the binding of ligand **5b** (Figure 5), interactions are similar to that as described for **5a** in Figure 3, except the 2-napthalene group extends deeper into the β-cavity. However, the larger size of this Ar group limits somewhat the conformational versatility (ω dihedral angle) of the ligand, and it has much fewer poses compared to either **5a** and **5c** (Table 3). For **5c**, the orientation of the 1-napthalene allows for greater conformational flexibility in the GPb binding site compared to its 2-napthalene equivalent, and indeed the **t3** tautomer is able to adopt a pose (ω = -154.9°; Table 3) similar to that shown for **5a** in Figure 3, with a flip in the 1,2,4-triazole.

Figure 3. The lowest solution phase energy pose of ligand **5a** (tautomer **t2**) bound at GPb with a dihedral angle ($\omega = 19.7°$; Table 3), as calculated using QM/MM and described in the text.
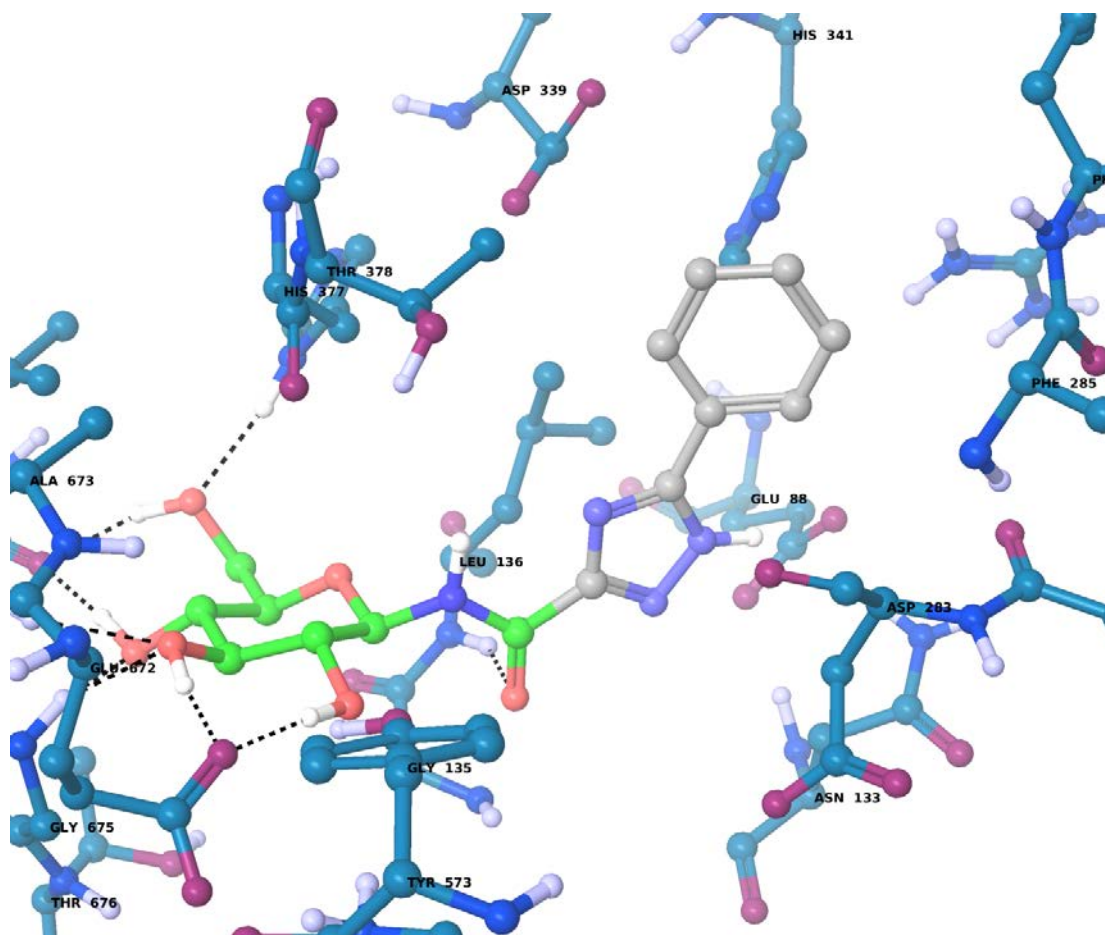
Figure 4. The flipped 1,2,4-triazole binding conformation of tautomer **t2** of **5a** at GPb (dihedral angle ω = -176.7°; Table 3), as calculated using QM/MM and described in the text. The tautomeric **t2** state allows for favorable intra-molecular hydrogen bond contacts between the carboxamide NH and a 1,2,4-triazole N when ω is close to 0° (Figure 2) or flipped (above). In the flipped conformation, the 1,2,4-triazole NH is close to hydrogen bonding distance with the Glu88 carboxylate.
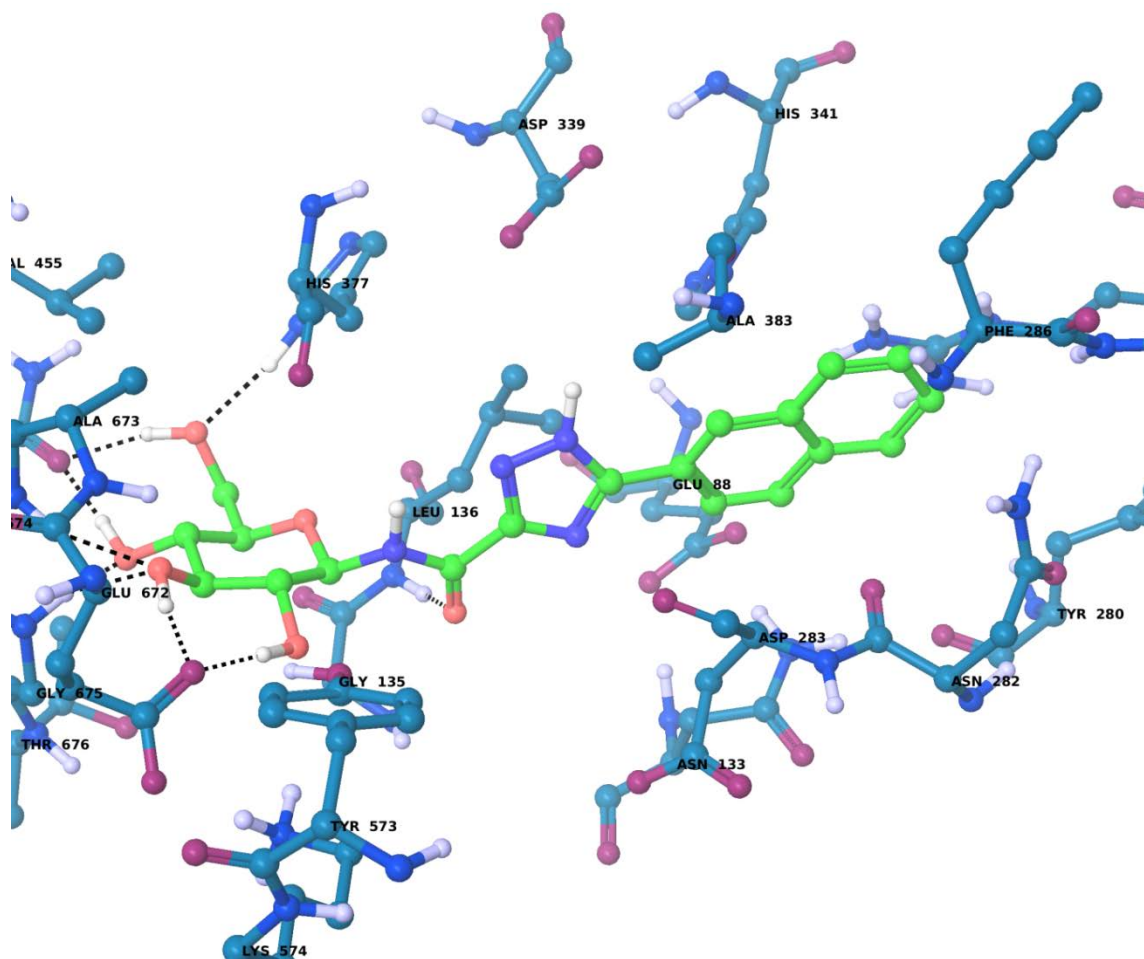
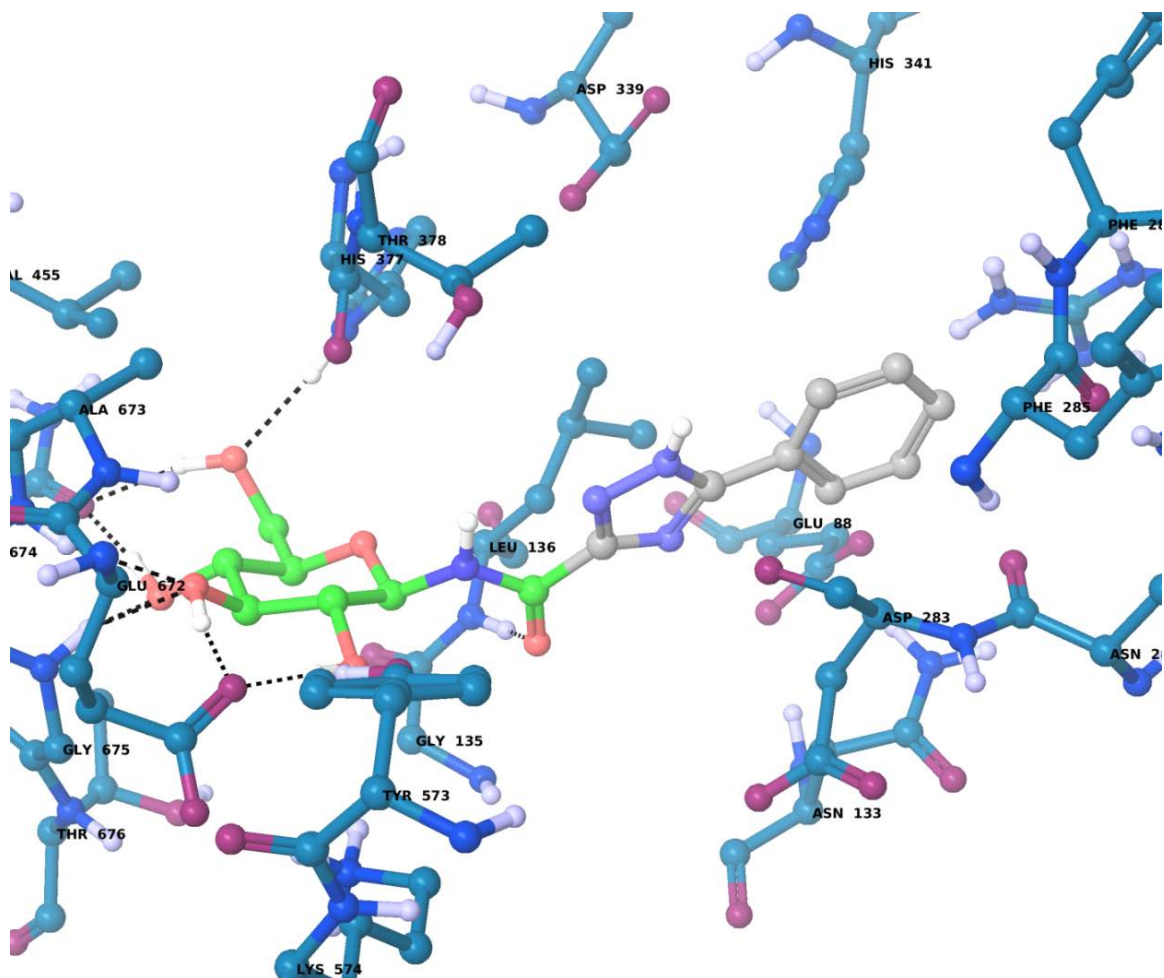**Figure 5**. The lowest solution phase energy pose of ligand **5b** (tautomer **t2**) bound at GPb (dihedral angle ω = -10.1˚; Table 3), calculated using QM/MM as described in the text.

Synthesis

Based on the computational results, synthesis of the ligands was considered worthwhile.
Several methods have been published for the preparation of 3,5-disubstituted 1,2,4-triazoles.[37]
While acyl-amidrazones (prepared from amides, thioamides, nitriles, or amidines) could be
transformed into the desired triazoles under thermal conditions, [37-39] the cycloaddition of
nitriles with nitrile-imines or nitrile-iminium ions gave 2,3,5-trisubstituted 1,2,4-triazoles in
moderate to good yields.[40-43] The reaction of 5-substituted tetrazoles with imidoyl chlorides
(easily obtained from the corresponding amides by SOCl$_2$) gave 3,4,5-trisubstituted 1,2,4-
triazoles in good yields. [44, 45]

8a, 9a, 10a, 11a, 12a; 5b Ar = phenyl
8b, 9b, 10b, 11b; 12b; 5b Ar = naphth-2-yl
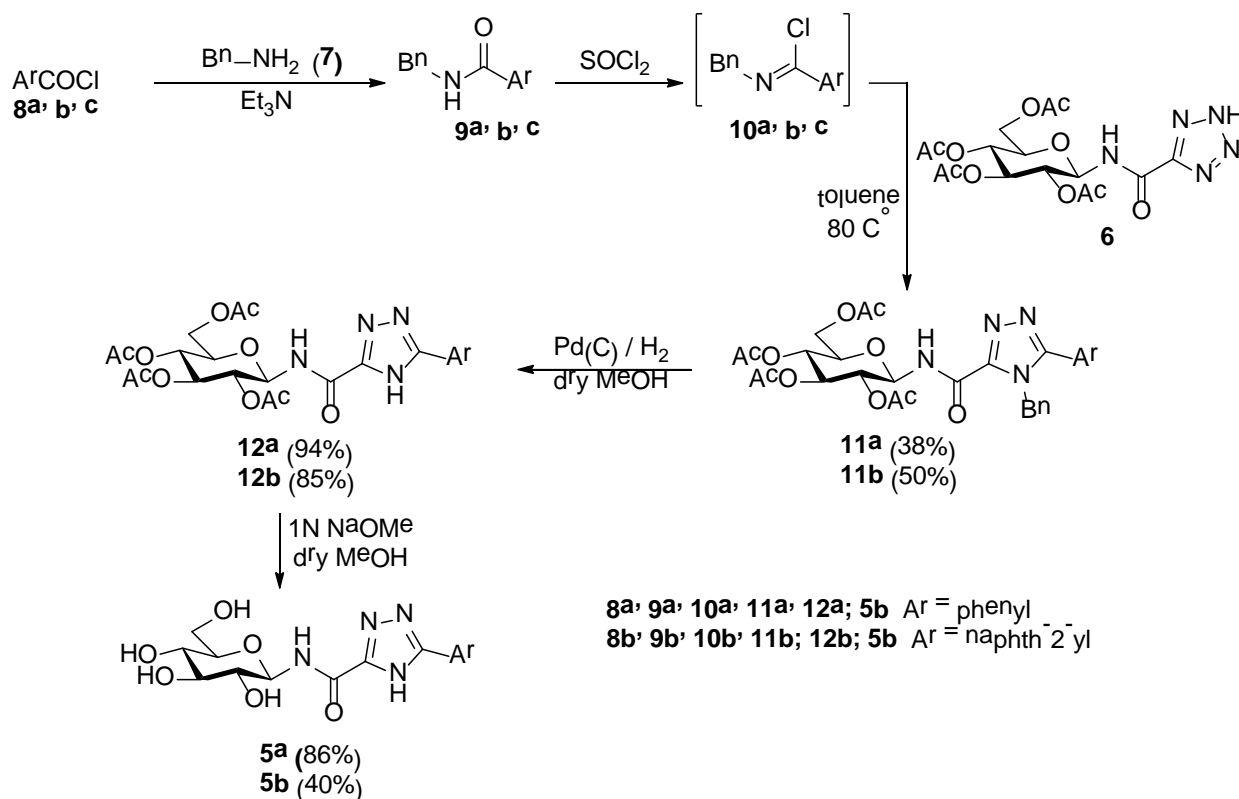
Scheme 1: Synthesis of the predicted molecules **5a,b**

This latter method was extensively applied for the preparation of 3-(*C*-glycosyl)-5-substituted-1,2,4-triazoles in our group.[13] The predicted target compounds of this study (**5a,b**) have been prepared using this methodology starting from tetrazole **6**[16] as shown in Scheme 1. The imidoyl chlorides **10a,b** and prepared from *N*-benzyl-amides **9a,b** as described earlier,[13] were reacted with tetrazole **6** without any purification to give the corresponding 4-benzyl-*N*-(2,3,4,6-tetra-*O*-acetyl-β-D-glucopyranosyl)-5-aryl-1,2,4-triazole-3-carboxamides **11a,b** in moderate yields. In the case of the 1-naphthyl derivative **5c**, the formation of **11c** from **10c** was unsuccessful, no transformation was detected and the desired compound has not been synthesized yet using any other synthetic methods.

The protecting groups were cleaved in a two-steps procedure. The *N*-benzyl group of **11a,b** was removed first by catalytic hydrogenation in excellent yields (94 and 85%). Subsequently, *O*-deacetylation was effected by the Zemplén method to give fully deprotected *N*-(β-D-glucopyranosyl)-5-aryl-1,2,4-triazole-3-carboxamides **5a,b**.

Enzyme kinetics

The inhibition constants (K_i) against rabbit muscle glycogen phosphorylase *b* (RMGP*b*) of compounds **5a,b** were determined according to the protocol described earlier [46]. The results are summarized in Table 1 together with the K_i's of 1,2,4- and 1,3,4-oxadiazole-carboxamide type inhibitors. As the data shows, the 1,2,4-triazole analogues **5a** ($K_i = 1$ μM) and **5b** ($K_i = 9.2$ μM) are more potent inhibitors than the oxadiazole analogues, consistent with our computational predictions for favorable binding at GPb.

Pharmacokinetic Predictions

The early evaluation of the pharmacokinetic properties of lead compounds in drug design efforts is desirable due to the potential for failure in late stage clinical trials. Accordingly, the absorption, distribution, metabolism and excretion (ADME) properties of **5a**-**5c** were predicted using the QikProp 3.5 program in normal mode.[18] Toxicity is the leading cause of drug attrition in clinical trials, together with lack of efficacy.[47] The FAF-Drugs2 server was used to extract any potential toxicity structural warnings.[48] Results are shown in Table 4.

An orally active drug should have no more than one violation of Lipinski's 'rule of five',[49] while for Jorgensen's 'rule of three' [50, 51] more drug-like molecules have fewer violations. The *N*-(β-D-glucopyranosyl)-1,2,4-triazolecarboxamides **5a**-**5c** had only one violation of each. The Lipinski violation is due to too many hydrogen bond donors (HBDs), 6 instead of ≤ 5 in each case, but this is still within the range for 95% of known drugs and consistent with some recent 'beyond rule of five' studies.[52, 53] In terms of Jorgensen's rules, the Caco-2 cell permeability (> 22 nm s^{-1}) is violated for the ligands (~ 19 nm s^{-1}), where previously we noted that the sensitive balance between adequate lipophilicity and solubility may need attention in lead optimization of heterocyclic derivatives conjugated to glucose[16]. Meanwhile, the log K_{hsa}'s (degree of human serum albumin affecting bioavailability) is ~ -0.9 – -0.7 and within the range for 95% of known drugs (-1.5 – 1.5), while the log BB (blood-brain barrier coefficients) values (-2.9 – -2.8) are also within the desirable range (-3.0 – 1.2). Importantly, there were no toxicity structural warnings for the ligands from FAF-Drugs2. Overall, the pharmacokinetic results are similar with the results for the *N*-(β-D-glucopyranosyl)-oxadiazole-carboxamides previously reported.[16] However, in terms of pharmacodynamics the **5a,b** ligands proved via kinetics experiments to be much more potent inhibitors of GP.

Table 4. Results of ADMET property predictions for the different tautomers of the *N*-(β-D-glucopyranosyl)-1,2,4-triazolecarboxamides inhibitors (**5a**-**5c**) studied in this work.[a]

Inhibitor/ tautomer	Lipinski's Rule of Five and Violations (V)[b]					Jorgensen's Rule of Three and Violations (V)[b]				PSA [Å²][c]	log K_{hsa}[d]	log *BB*[e]	TSW[f]
	M_r [Da] (<500)	HBD[g] (≤5)	HBA[h] (≤10)	log $P_{(o/w)}$ (<5)	V	Caco-2 [nm s⁻¹][i] (>22)	log *S* (>-5.7)	NMP[j] (<7)	V	(<140 Å²)			
5a													
t1	350.3	*6*	10	-1.6	1	*19.2**	-2.7	5	1	*173.3*	-1.02	-2.8	-
t2	350.3	*6*	10	-1.1	1	*19.2**	-2.8	5	1	*173.3*	-0.93	-2.8	-
t3	350.3	*6*	10	-1.4	1	*18.9**	-2.8	5	1	*173.4*	-0.97	-2.8	-
5b													
t1	400.4	*6*	10	-0.8	1	*19.2**	-3.4	5	1	*173.3*	-0.85	-2.9	-
t2	400.4	*6*	10	-0.3	1	*19.2**	-3.6	5	1	*173.2*	-0.72	-2.9	-
t3	400.4	*6*	10	-0.6	1	*19.0**	-3.6	5	1	*173.4*	-0.80	-2.9	-
5c													
t1	400.4	*6*	10	-0.8	1	*18.2**	-3.4	5	1	*174.7*	-0.85	-2.9	-
t2	400.4	*6*	10	-0.4	1	*18.8**	-3.6	5	1	*174.2*	-0.72	-2.9	-
t3	400.4	*6*	10	-0.7	1	*18.3**	-3.5	5	1	*174.6*	-0.80	-2.9	-
Range[k]	**130-725**	**0-6**	**2-20**	**-2.0-6.5**	**-**	**<25 poor; > 500 great**	**-6.5-0.5**	**1-8**	**-**	**7-200**	**-1.5-1.5**	**-3.0-1.2**	**-**

[a] ADMET data calculated using Qikprop 3.5[18]; predicted properties outside the range for 95% of known drugs indicated with an asterisk (*). [b] Rules as listed in the columns, with any violations of the rules highlighted in *italics*. [c] PSA represents the van der Waals (polar) surface areas of N and O atoms; recommended PSA <140 Å² according to Veber et al.[54] [d] log K_{hsa}: predicted binding to human serum albumin. [e] log *BB*: predicted blood-brain barrier coefficient. [f] Toxicity structural warnings from FAF-Drugs2.[48] [g] Number of hydrogen bond donors. [h] Number of hydrogen bond acceptors. [i] Caco-2 cell permeability. [j] Number of primary metabolites. [k] Range for 95% of known drugs.[18]

Experimental

Computational details (additional)

Free ligand calculations: To determine the important (low energy) tautomeric forms/conformations of the model ligands **5** (Table 2), 1000 steps of the Monte Carlo Multiple Minima (MCMM) method were performed using MacroModel 9.9,[18] the OPLS-AA(2005) forcefield[33] and GB/SA continuum model for H_2O solvation effects.[55] The conformations were then optimized using DFT (M06-2X/6-31+G*) with Jaguar 8.0[18] and frequency calculations used to characterize the stationary points as true minima, as well as for calculation of the gas-phase Gibbs free energies at 298.15 K. For the solution phase QM calculations (M06-2X/cc-pVTZ++) [22] at these geometries, a SCRF continuum treatment of solvation with the PBF equation was used.[24, 25]

Protein Preparation: The initial setup of the GPb receptor for calculations was performed using Schrodinger's "Protein Preparation Wizard"[18] starting from the GPb–**1b** co-crystallised complex. Water molecules were deleted, bond orders assigned, and hydrogen atoms added, with protonation states for basic and acidic residues based on residue pK_a values at normal pH (7.0). Subsequent optimization of hydroxyl groups, histidine protonation states and C/N atom "flips", and side-chain O/N atom flips of Asn and Gln was based on optimizing hydrogen bonding patterns. The phosphate in pyridoxal-phosphate (PLP) was assigned in monoanionic form. Finally, an "Impref" minimization of the GPb complex was performed using the OPLS-AA(2005) force field[33] to remove steric clashes and bad contacts but with heavy atoms constrained to within 0.3 Å (RMSD) of their crystallographic positions.

Docking Details: For the Glide 5.8 docking calculations in extra-precision (XP) mode, the shape and properties of the GPb catalytic binding site were first mapped onto grids with dimensions of ~26.7 × 26.7 × 26.7 Å centred on the native co-crystallized ligand (**1b**). Core constraints (1 Å) on the six glucose ring atoms + the ligands' amide moieties to retain them

close to the native ligand crystallographic positions were applied. Post-docking minimization of the ligand poses was performed (with strain correction) with a maximum of 5 poses per ligand saved. Poses were considered conformationally distinct for RMSDs (heavy atoms) > 0.5 Å.

Synthesis

The general procedures employed for the synthesis are described in the ESI, together with the NMR data.

GP Inhibition Assay

Glycogen phosphorylase b was prepared from rabbit skeletal muscle according to the method of Fischer and Krebs[56] using 2-mercaptoethanol instead of L-cysteine, and recrystallized at least three times before use. The kinetic studies with glycogen phosphorylase were performed as described previously.[46] Kinetic data for the inhibition of rabbit skeletal muscle glycogen phosphorylase by monosaccharide compounds were collected using different concentrations of α-D-glucose-1-phosphate (4, 6, 8, 10, 12 and 14 mM) and constant concentrations of glycogen (1% w/v) and AMP (1 mM). The enzymatic activities were presented in the form of double-reciprocal plots (Lineweaver–Burk) applying a nonlinear data-analysis programme. The inhibitor constants (K_i) were determined by Dixon plots, by replotting the slopes from the Lineweaver–Burk plots against the inhibitor concentrations. The means of standard errors for all calculated kinetic parameters averaged to less than 10%. [3, 57] IC_{50} values were determined in the presence of 4 mM glucose 1-phosphate, 1 mM AMP, 1% glycogen, and varying concentrations of an inhibitor.

Conclusions

Molecular modeling investigations in the form of docking, QM and QM/MM studies has motivated the experimental evaluation of *N*-(β-D-glucopyranosyl)-1,2,4-triazolecarboxamides as GP inhibitors. The value of QM calculations to determine favorable tautomeric states is highlighted, while QM/MM optimizations were used to decipher the more likely binding interactions in the absence of time consuming X-ray crystallographic evidence. While there is often uncertainty in assigning hydrogen positions using crystallography,[58] QM/MM calculations allowed us to accurately consider the binding potential of the different **5a**-**5c** 1,2,4-triazole tautomers, with the GPb interactions formed by the most stable **t2** tautomer and its conformational flexibility deemed significant. Synthesis, followed by kinetics experiments revealed **5a,b** as low µM inhibitors of GP, with **5a** the in the top 10 most potent catalytic site inhibitor discovered to date.[4] The *N*-(β-D-glucopyranosyl)-1,2,4-triazolecarboxamides are predicted to have drug-like potential, but with permeability a potential issue to efficacy. While intra-molecular bonding has the potential to improve membrane permeability by reducing the polar surface areas,[52] this effect is likely to be minimal in our case. However, glucose analogues have already demonstrated blood glucose lowering effects *in vivo*, [10, 11] a large number of triazole compounds are found as clinical drugs or candidates for treatment of a range of diseases[59], so that we consider the ligands studied worthy candidates for further optimization studies. Finally, the value of a computationally lead approach to GP inhibitor design has been highlighted in this work.[27]

References

1. G. Danaei, M. M. Finucane, Y. Lu, G. M. Singh, M. J. Cowan, C. J. Paciorek, J. K. Lin, F. Farzadfar, Y.-H. Khang, G. A. Stevens, M. Rao, M. K. Ali, L. M. Riley, C. A. Robinson, M. Ezzati and C. Global Burden Metab Risk Factors, *Lancet*, 2011, **378**, 31-40.
2. M. Brownlee, *Nature*, 2001, **414**, 813-820.
3. N. G. Oikonomakos, *Curr. Protein Pept. Sci.*, 2002, **3**, 561-586.
4. J. M. Hayes, A. L. Kantsadi and D. D. Leonidas, *Phytochem. Rev.*, 2014, **13**, 471-498.
5. L. Somsák, K. Czifrák, M. Tóth, É. Bokor, E. D. Chrysina, K. M. Alexacou, J. M. Hayes, C. Tiraidis, E. Lazoura, D. D. Leonidas, S. E. Zographos and N. G. Oikonomakos, *Curr. Med. Chem.*, 2008, **15**, 2933-2983.
6. E. D. Chrysina, M. N. Kosmopolou, C. Tiraidis, R. Kardarakis, N. Bischler, D. D. Leonidas, Z. Hadady, L. Somsák, T. Docsa, P. Gergely and N. G. Oikonomakos, *Protein Sci.*, 2005, **14**, 873-888.
7. A. L. Kantsadi, A. Apostolou, S. Theofanous, G. A. Stravodimos, E. Kyriakis, V. A. Gorgogietas, D. S. M. Chatzileontiadou, K. Pegiou, V. T. Skamnaki, D. Stagos, D. Kouretas, A.-M. G. Psarra, S. A. Haroutounian and D. D. Leonidas, *Food Chem. Toxicol.*, 2014, **67**, 35-43.
8. L. Somsák, É. Bokor, K. Czifrák, L. Juhász and M. Tóth, in *Topics in the Prevention, Treatment and Complications of Type 2 Diabetes*, ed. M. B. Zimering, InTech Open Access Publisher, Rijeka, 2011, pp. 103-126.
9. L. Somsák, *Compt. Rend. Chimie*, 2011, **14**, 211-223.
10. T. Docsa, K. Czifrák, C. Hüse, L. Somsák and P. Gergely, *Mol. Med. Rep.*, 2011, **4**, 477-481.
11. L. Nagy, T. Docsa, A. Brunyánszki, M. Szántó, C. Hegedős, J. Marton, B. Kónya, L. Virág, L. Somsák, P. Gergely and P. Bai, *PLoS ONE*, 2013, **8**, e69420.
12. V. Nagy, K. Czifrák, A. Bényei and L. Somsák, *Carbohydr. Res.*, 2009, **344**, 921-927.
13. S. Kun, É. Bokor, G. Varga, B. Szőcs, A. Páhi, K. Czifrák, M. Tóth, L. Juhász, T. Docsa, P. Gergely and L. Somsák, *Eur. J. Med. Chem.*, 2014, **76**, 567-579.
14. É. Bokor, T. Docsa, P. Gergely and L. Somsák, *ACS Med. Chem. Lett.*, 2013, **4**, 612-615.
15. M. Benltifa, J. M. Hayes, S. Vidal, D. Gueyrard, P. G. Goekjian, J.-P. Praly, G. Kizilis, C. Tiraidis, K.-M. Alexacou, E. D. Chrysina, S. E. Zographos, D. D. Leonidas, G. Archontis and N. G. Oikonomakos, *Bioorg. Med. Chem.*, 2009, **17**, 7368-7380.
16. M. Polyák, G. Varga, B. Szilágyi, L. Juhász, T. Docsa, P. Gergely, J. Begum, J. M. Hayes and L. Somsák, *Bioorg. Med. Chem.*, 2013, **21**, 5738-5747.
17. Y.-C. Cheng and W. H. Prusoff, *Biochem. Pharmacology*, 1973, **22**, 3099-3108.
18. Schrodinger, LLC, New York, NY, 2014.
19. Y. Zhao and D. G. Truhlar, *Theor. Chem. Acc.*, 2008, **120**, 215-241.
20. M. M. Francl, W. J. Pietro, W. J. Hehre, J. S. Binkley, M. S. Gordon, D. J. Defrees and J. A. Pople, *J. Chem. Phys.*, 1982, **77**, 3654-3665.
21. W. J. Hehre, R. Ditchfield and J. A. Pople, *J. Chem. Phys.*, 1972, **56**, 2257-2261.
22. D. E. Woon and T. H. Dunning, *J. Chem. Phys.*, 1993, **98**, 1358-1371.
23. E. Arunan, G. R. Desiraju, R. A. Klein, J. Sadlej, S. Scheiner, I. Alkorta, D. C. Clary, R. H. Crabtree, J. J. Dannenberg, P. Hobza, H. G. Kjaergaard, A. C. Legon, B. Mennucci and D. J. Nesbitt, *Pure Appl. Chem.*, 2011, **83**, 1637-1641.

24. D. J. Tannor, B. Marten, R. Murphy, R. A. Friesner, D. Sitkoff, A. Nicholls, M. Ringnalda, W. A. Goddard and B. Honig, *J. Am. Chem. Soc.*, 1994, **116**, 11875-11882.
25. B. Marten, K. Kim, C. Cortis, R. A. Friesner, R. B. Murphy, M. N. Ringnalda, D. Sitkoff and B. Honig, *J. Phys. Chem.*, 1996, **100**, 11775-11788.
26. R. A. Friesner, R. B. Murphy, M. P. Repasky, L. L. Frye, J. R. Greenwood, T. A. Halgren, P. C. Sanschagrin and D. T. Mainz, *J. Med. Chem.*, 2006, **49**, 6177-6196.
27. J. M. Hayes and D. D. Leonidas, *Mini-Rev. Med. Chem.*, 2010, **10**, 1156-1174.
28. A. L. Kantsadi, J. M. Hayes, S. Manta, V. T. Skamnaki, C. Kiritsis, A.-M. G. Psarra, Z. Koutsogiannis, A. Dimopoulou, S. Theofanous, N. Nikoleousakos, P. Zoumpoulakis, M. Kontou, G. Papadopoulos, S. E. Zographos, D. Komiotis and D. D. Leonidas, *ChemMedChem*, 2012, **7**, 722-732.
29. G. Carta, A. J. S. Knox and D. G. Lloyd, *J. Chem. Inf. Model.*, 2007, **47**, 1564-1571.
30. S. Zhong, Y. Zhang and Z. Xiu, *Curr. Opin. Drug Discov. Devel.*, 2010, **13**, 326-334.
31. P. Pospisil, P. Ballmer, L. Scapozza and G. Folkers, *J. Recept. Sig. Transd.*, 2003, **23**, 361-371.
32. A. E. Cho, J. Y. Chung, M. Kim and K. Park, *J. Chem. Phys.*, 2009, **131**.
33. G. A. Kaminski, R. A. Friesner, J. Tirado-Rives and W. L. Jorgensen, *J. Phys. Chem. B*, 2001, **105**, 6474-6487.
34. J. S. Murray, S. Ranganathan and P. Politzer, *J. Org. Chem.*, 1991, **56**, 3734-3737.
35. J. S. Murray and P. Politzer, *J. Org. Chem.*, 1991, **56**, 6715-6717.
36. P. W. Kenny, *J. Chem. Inf. Model.*, 2009, **49**, 1234-1244.
37. J. B. Polya, in *Comprehensive Heterocyclic Chemistry*, 1984, vol. 5, pp. 733-790.
38. K. T. Potts, *J. Chem. Soc., Dalton Trans.*, 1954, 3461-3464.
39. K. T. Potts, *Chem. Rev.*, 1961, **61**, 87-127.
40. R. Huisgen, J. Sauer and M. Seidel, *Chemische Berichte*, 1961, **94**, 2503-2509.
41. R. Huisgen, R. Grashey, M. Seidel, G. Wallbillich, H. Knupfer and R. Schmidt, *Liebigs Annalen der Chemie*, 1962, **653**, 105-113.
42. S. Condi, C. Corral and R. Madronero, *Synthesis*, 1974, 28-29.
43. G. Broggini, L. Bruche, L. Garanti and G. Zecchi, *J. Chem. Soc., Perkin Trans. 1*, 1994, 433-438.
44. R. Huisgen, J. Sauer and M. Seidel, *Chemische Berichte*, 1960, **93**, 2885-2891.
45. G. I. Koldobskii and V. A. Ostrovskii, *Russ. Chem. Rev. (Engl. Transl.)*, 1994, **63**, 797.
46. E. Ősz, L. Somsák, L. Szilágyi, L. Kovács, T. Docsa, B. Tóth and P. Gergely, *Bioorg. Med. Chem. Lett.*, 1999, **9**, 1385-1390.
47. G. F. Smith, *Prog. Med. Chem.*, 2011, **50**, 1-47.
48. D. Lagorce, J. Maupetit, J. Baell, O. Sperandio, P. Tuffery, M. A. Miteva, H. Galons and B. O. Villoutreix, *Bioinformatics*, 2011, **27**, 2018-2020.
49. C. A. Lipinski, F. Lombardo, B. W. Dominy and P. J. Feeney, *Adv. Drug Deliv. Rev.*, 1997, **23**, 3-25.
50. W. L. Jorgensen and E. M. Duffy, *Bioorg. Med. Chem. Lett.*, 2000, **10**, 1155-1158.
51. W. L. Jorgensen and E. M. Duffy, *Adv. Drug Deliv. Rev.*, 2002, **54**, 355-366.
52. A. Alex, D. S. Millan, M. Perez, F. Wakenhut and G. A. Whitlock, *MedChemComm*, 2011, **2**, 669-674.
53. G. V. Paolini, R. H. B. Shapland, W. P. van Hoorn, J. S. Mason and A. L. Hopkins, *Nat. Biotechnol.*, 2006, **24**, 805-815.
54. D. F. Veber, S. R. Johnson, H. Y. Cheng, B. R. Smith, K. W. Ward and K. D. Kopple, *J. Med. Chem.*, 2002, **45**, 2615-2623.
55. W. C. Still, A. Tempczyk, R. C. Hawley and T. Hendrickson, *J. Am. Chem. Soc.*, 1990, **112**, 6127-6129.

56.   E. H. Fischer and E. G. Krebs, *Methods in Enzymology*, 1962, **5**, 369-372.
57.   L. Somsák, L. Kovács, M. Tóth, E. Ősz, L. Szilágyi, Z. Györgydeák, Z. Dinya, T. Docsa, B. Tóth and P. Gergely, *J. Med. Chem.*, 2001, **44**, 2843-2848.
58.   R. Lonsdale, J. N. Harvey and A. J. Mulholland, *Chem. Soc. Rev.*, 2012, **41**, 3025-3038.
59.   C. H. Zhou and Y. Wang, *Curr. Med. Chem.*, 2012, **19**, 239-280.